International Journal of Microwave and Wireless Technologies

cambridge.org/mrf

Novel sunflower MIMO fractal antenna with low mutual coupling and dual wide operating bands

Amer T. Abed

Communication Engineering Department, Al-Ma'moon University College, 14th Ramadan street, Baghdad, Iraq

Research Paper

Cite this article: Abed AT (2020). Novel sunflower MIMO fractal antenna with low mutual coupling and dual wide operating bands. *International Journal of Microwave and Wireless Technologies* **12**, 323–331. https://doi.org/10.1017/S1759078719001375

Received: 30 December 2018
Revised: 22 September 2019
Accepted: 25 September 2019
First published online: 30 October 2019

Key words:
Fractal; LTE and 5G; MIMO antenna; mutual coupling

Author for correspondence:
Amer T. Abed, E-mail: amer.t.abed@ieee.org

Abstract

A novel multiple-input and multiple-output (MIMO) fractal antenna excited by a coplanar waveguide was investigated in this study. A novel technique was used to improve the isolation of 20 dB between the dual radiating elements by inserting a strip line into the outer edges of the ground plane. A sunflower structure was used to configure the antenna in three steps. At each step, an additional sunflower structure was added with half the size of that used in the previous step to enhance the impedance bandwidth. The measured values of envelop correlation coefficient and total active reflection coefficient indicated that the proposed MIMO antenna has high-diversity performance between radiating elements. Wide dual operating bands of 2–2.9 and 5–10 GHz were obtained, which can support different wireless communications, such as 3G, LTE (2.6 GHz), WLAN (2.4 GHz/5 GHz), WiMAX (2.4 GHz/5GHz), ISM (2.4 GHz/5 GHz), 5G (5–6 GHz), and satellite communications (6–8 GHz). The MIMO fractal antenna with a small size achieved a maximum efficiency of 85% and a peak value gain of 6 dBi, low-channel capacity loss of 0.15–0.4 b/s/Hz, and high isolation between radiating elements is suitable for portable communication devices.

Introduction

At present, modern communication networks, such as Wi-Fi, 3G, WiMAX (4G), and LTE use multiple-input and multiple-output (MIMO) antennas to improve wireless channel capacity and provide effective and high-data rates [1]. In MIMO technology, data are simultaneously transmitted and received in the same channel [1]. Many studies have designed MIMO antennas using different geometries (patch, slot, and fractal) with various types of feed, e.g., strip, coaxial, and coplanar waveguide (CPW) lines. Examples include the antennas reported in [2–31]. Table 1 lists the weakness of related antennas previously investigated in [2–31]. The table also presents important characteristics, such as number of elements (No. El), impedance bandwidth, efficiency, gain, mutual coupling (S_{ij}), and size. Previous MIMO antennas were either too large such that they cannot be used in modern portable communication devices [2, 6, 7, 8, 13, 14, 16, 17, 19, 20, 21, 29, 30], or small but cannot support the requirements of modern communication networks, such as 3G, WLAN, LTE, and WiMAX [3, 10, 12, 15, 18, 22, 23, 25, 27, 28].

The mutual effect among the radiating elements in an antenna, which is called mutual coupling, is crucial in designing MIMO antennas. Many techniques used to improve the isolation between radiating elements such as: split-ring resonator with 17 dB mutual coupling reduction [11], placing orthogonally planar inverse-F antennas with mutual coupling reduction of 20 dB [13], T-shape parasitic element [15] or parasitic strip line [30] to improve the isolation between the radiating elements by 10 dB, using a neutralization line with mutual coupling reduction of 15 dB [22], and etching Amer fractal slot in the radiator plane to reduce the mutual coupling 10 dB [31].

A mutual coupling of <−20 dB is preferred [19]. The antennas listed in Table 1 exhibit mutual coupling greater than −20 dB, except for those investigated in [4, 8, 17 18, 19, 23, 28]. However, the antennas reported in [8, 17, 19] had a large size, whereas those studied in [4, 18, 23, 28] do not support all the required spectra.

Based on Table 1 and literature review, it is needed to design a MIMO antenna which must support the requirements of modern wireless communications, such as 3G, LTE (2.6 GHz), WLAN (2.4 GHz/5 GHz), WiMAX (2.4 GHz/5 GHz), ISM (2.4 GHz/5 GHz), and 5G (5–6 GHz). An antenna must have low-mutual coupling, low-channel capacity loss (CCL), acceptable values of gain and efficiency, and a small size.

This research aims to design a MIMO fractal antenna with low-mutual coupling between radiating elements that can be used for 3G, LTE (4G), WLAN (IEEE 802.11n and IEEE 802.11ac), WiMAX (IEEE 802.16), ISM, and 5G (5–6 GHz) communication devices and that exhibits high efficiency and acceptable gain values in a small size suitable for portable devices.

CAMBRIDGE UNIVERSITY PRESS

Table 1. Comparison of antennas investigated in [2–31]

Ref.	No. El.	B.W (GHz)	Effie. %	Gain (dB)	Mutual coupling (dB)	Size (mm^3)	Weakness
[2]	4	(2.3–2.9)	80–90	0–5	< – 10	91 × 91 × 0.8	Large size, does not support all required spectra
[3]	3	(5–6)	55–60	–2 to 2	< – 15	48 × 29 × 1.6	Low gain and efficiency at lower band, does not support all required spectra
[4]	2	(2.4–2.5) (5–6)	–	–	< – 25	77 × 34 × 0.8	There is no reports about values of gain and efficiency, cannot be used for 3G & LTE
[5]	2	(4–6.5)	80	4–7	< – 15	80 × 50 × 0.76	Cannot be used for 3G, LTE, and WLAN
[6]	4	(1.8–2.5)	51–73	–2.6 to 2.4	< – 10	120 × 60 × 0.7	Large size, missed many required frequencies, low gain & efficiency at lower band
[7]	4	(2.15–2.33)	75–85	–	< – 11	100 × 60 × 0.8	Large size, narrow BW, there is no reports about values of gain and efficiency
[8]	4	(27.5–28.5)	–	–	< – 30	130 × 70 × 2.2	Large size, efficiency and gain values are not reported, cannot be used for 3G, LTE, and WLAN
[9]	2	(0.95–1.02) (2.68–2.85) (4.20–4.40) (5.50–5.65)	–	2.5–6.5	< – 17	82 × 40 × 0.8	Narrow band around resonant frequencies. There is no reports about values of efficiency
[10]	2	(3–10.5)	40–82	2–5.5	< – 15	24.3 × 22 × 0.8	Cannot be used for 3G, LTE, and WLAN, low efficiency at lower band
[11]	2	(2.4–2.48) (5.15–5.825)	60–80	–	< – 15	77.5 × 52 × 1.6	Cannot be used for 3G & LTE, there is no gain values
[12]	4	(1.95–2.5) (3.15–3.85) (4.95–6.6)	60–80	–1 to 2	< – 15	40 × 40 × 1.6	Cannot be used for LTE, low gain at lower band
[13]	2	(1.8–2.5) (26–28.5)	–	1.5–3.5	< – 10	100 × 60 × 0.9	Large size, there is no reports about values efficiency, antenna does not support all required spectra
[14]	4	(2.6–2.8) (3.4–3.6)	–	2–4	< – 16	140 × 70 × 9.5	Large size, there is no reports about values efficiency, antenna did not support WLAN, WiMX, and 3G applications
[15]	4	(3–9)	60–85	0.5–2	< – 10	40 × 40 × 0.8	Antenna did not support 3G, LTE, WLAN, and WiMAX applications
[16]	2	(1.9–3.7)	–	–0.5 to 6	< – 15	100 × 50 × 1.6	Large size, there is no reports about values efficiency
[17]	2	(2.43–2.49)	–	–	<–20	100 × 80 × 1.6	Large size, narrow operating band, there is no reports about values of gain and efficiency
[18]	4	(2–5) (6–10)	–	–1.5 to 4	<–20	45 × 45 × 0.8	Missed many required frequencies, there is no reports about values of efficiency
[19]	2	(2.4–2.5) (5–6)	–	–	<–22	121 × 61 × 0.8	Large size, antenna does not support 3G & LTE, there is no reports about values of gain and efficiency
[20]	2	(1.6–1.9) (2.6–6.2)	88	–5 to 5	<–15	100 × 50 × 1.5	Large size, cannot be used for LTE & WLAN
[21]	2	(1.5–5.5) (5.1–5.8)	60	10–14	<–10	90 × 50 × 0.76	Large size, high-mutual coupling
[22]	2	(3–5) (6–11.8)	80	–4 to 4	<–15	38.5 × 38.5 × 1.6	Cannot be used for WLAN, LTE & WiMAX applications
[23]	2	(3.1–5)	70	2–3	<–22	35 × 33 × 0.8	Cannot be used for WLAN, LTE & WiMAX
[24]	2	(1.85–2.6)	85	–	<–15	80 × 80 × 1.6	Large size, missed many required frequencies
[25]	2	(2.4–2.48) (5.1–5.8)	–	–	<–14	56 × 20 × 1.6	Cannot be used for 3G & LTE applications, there is no reports about values of gain and efficiency

(*Continued*)

https://doi.org/10.1017/S1759078719001375 Published online by Cambridge University Press

Table 1. (*Continued.*)

Ref.	No. El.	B.W (GHz)	Effie. %	Gain (dB)	Mutual coupling (dB)	Size (mm^3)	Weakness
[26]	2	0.9/1.8/2.3/2.6	90	−2 to 4	<−10	80 × 60 × 0.8	Narrow operating bands around resonant frequencies, large size
[27]	2	(2.20–2.51)	–	−2.5 to 0.5	<−16	15.5 × 18 × 1.6	Cannot be used for LTE & WiMAX applications
[28]	2	(0.1–4.3)	56	−1 to 3.1	<− 25	8 × 8 × 0.8	Missed many required spectrum, low efficiency
[29]	4	(1.73–2.28)	51–75	−6 to 2.3	<−15	110 × 50 × 1.5	Large size, cannot be used for LTE, WLAN, and WiMAX applications, low gain at lower band
[30]	2	(2.35–2.5)	46–60	–	<−10	100 × 65 × 1.6	Large size, cannot be used for 3G, LTE, and WiMAX applications
[31]	4	(1.5–30)	45–80	1.3–6	<−10	33 × 33 × 0.8	Low mutual coupling at lower operating band between the neighbor ports

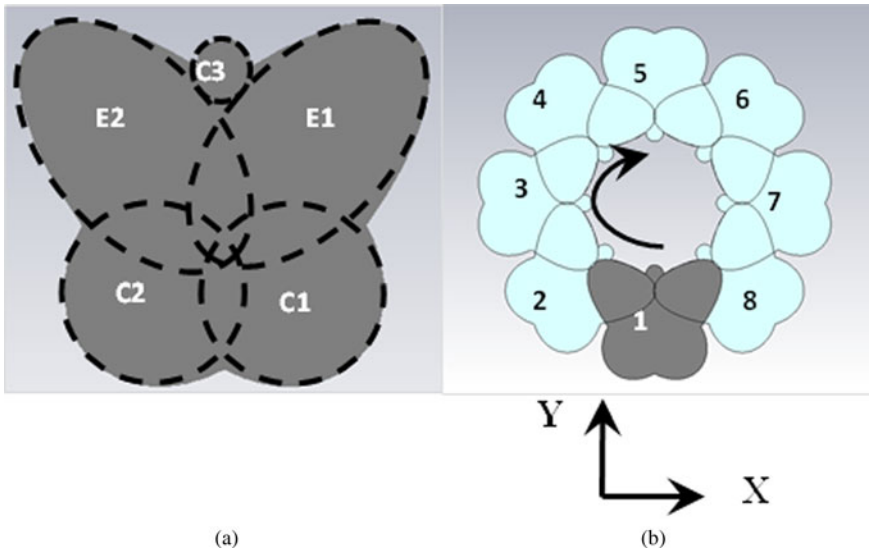

Fig. 1. Configuring the sunflower. (a) The initial structure. (b) The sunflower.

Antenna design and analysis

Antenna design

In this research, the initial metallic structure shown in Fig. 1(a) is configured by collecting dual elliptical shapes E_1 and E_2 (both of them have a major axis of 4 mm and a minor axis of 2 mm) with circular shapes C_1 and C_2 (both of them have a radius of 1.6 mm) and C_3 (with a radius of 0.5 mm). This process is repeated in a cycle with a radius of 9 mm at an angle of 45° (in the X–Y plane), the reference is the Y axis, which passes through the center of leave 1 to configure the sunflower structure; the structure consists of eight initial structures (the sunflower has eight vase leaves), as shown in Fig. 1(b).

The dimensions of the sunflower MIMO fractal antenna etched on an FR-4 substrate were $50 \times 40 \times 0.8$ mm^3. Figure 2(a) shows that the initiator antenna consisted of dual short radiators F with dimensions of 5.5×2 mm^2 located on opposite sides of the substrate to reduce mutual coupling among MIMO elements. The initiator antenna fed by CPW, gap g separates radiator F from the ground plates on the same side of the FR-4 substrate (Fig. 2(a)). Table 2 presents all the dimensions of the ground. The 1st iteration antenna was configured by adding the sunflower structure to both elements of the proposed MIMO antenna (Fig. 2(b)). The same process was repeated in the 2nd and the 3rd iterations, wherein the size of the added sunflower is half that in the previous iteration, as shown in Figs 2(c) and 2(d). The above transformation of the sunflower to generate any order of iterations can be represented by the mathematical formula [32]:

$$W\begin{bmatrix} x \\ y \end{bmatrix} = \begin{bmatrix} r\cos\theta & -s\cos\emptyset \\ r\sin\theta & s\sin\emptyset \end{bmatrix}\begin{bmatrix} x \\ y \end{bmatrix} + \begin{bmatrix} x_0 \\ y_0 \end{bmatrix} \quad (1)$$

where r and s are the scale factor, θ and $\emptyset$ are the rotation angles, and x_0 and y_0 are the amounts of translation. Since the additional sunflower structure at any iteration is half size of that used in the previous step, the factors r and s are reductions and equal to 0.5. The rotation angels θ and $\emptyset$ equal to zero. The amount of translation y_0 equals to 13.5 mm for the 2nd iteration and 20 mm for the 3rd iteration, while the amount of x_0 equals to zero at all iterations because the transformation of the sunflower structure in the Y-direction only.

Antenna analysis

Figure 3 presents the enhancement in impedance bandwidth during the process of the antenna configuration. The black dashed curve represents non-useful impedance bandwidth for the initiator

https://doi.org/10.1017/S1759078719001375 Published online by Cambridge University Press

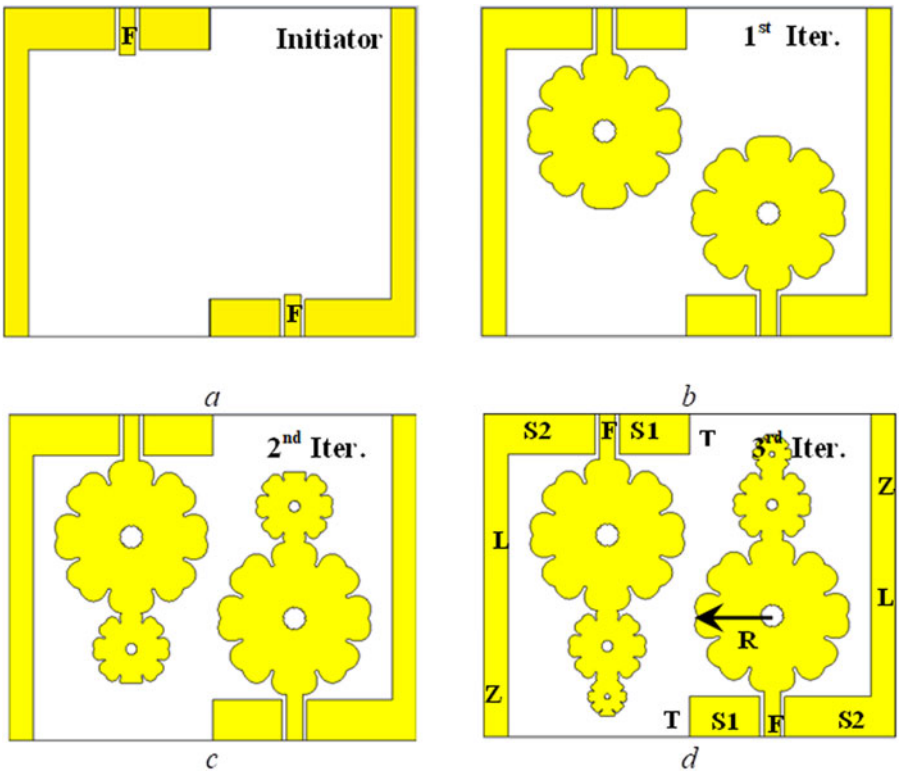

Fig. 2. The process of configuring sunflower MIMO fractal antenna.

Table 2. The dimensions of sunflower MIMO antenna

Parameter	(mm)	Parameter	(mm)
T	5	S_1	8.4
g	0.5	S_2	10.5
Z	3	R	9
L	25		

antenna. The effective area (A_e) increases with the addition of the sunflower structure in the first iteration, leading to increased gain and efficiency, according to equations (2) and (3) [33].

$$D = \frac{4\pi A_e}{\lambda^2} \tag{2}$$

$$\text{Efficiency} = \frac{\text{G}}{\text{D}} \tag{3}$$

where G is the gain, D is the directivity, and λ is the wavelength.

The operating band of the proposed MIMO antenna improved dramatically by adding the sunflower structure at the 1st iteration, where the dual operating bands of 2.6–7.1 and 7.5–12 GHz were observed (blue curve in Fig. 3), which missed many required frequencies for WLAN, LTE, and WiMAX applications. At the 2nd iteration (red curve in Fig. 3), dual operating bands were obtained at 2.5–3 and 5.5–12 GHz, with a fractional impedance bandwidth of 9 and 37% respectively.

The desired operating band was achieved at the 3rd iteration where the dual impedance bandwidths of 2.1–2.74 and 5–12 GHz were observed (the black curve in Fig. 3) with an impedance

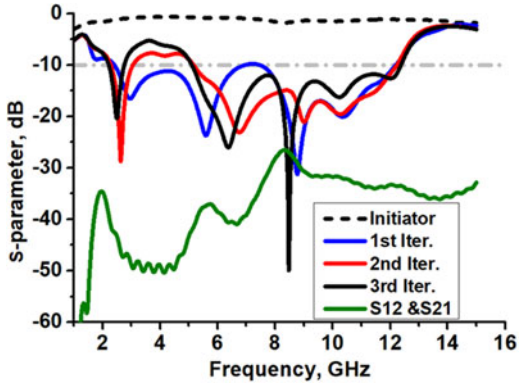

Fig. 3. Simulated *S*-parameters for all iterations.

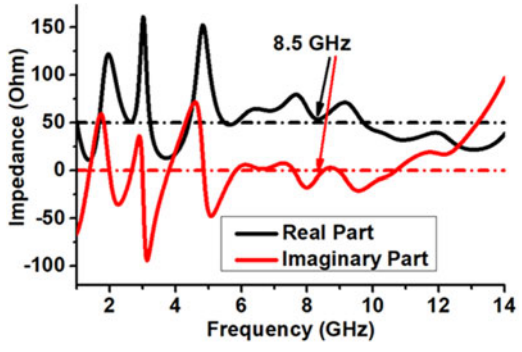

Fig. 4. Simulated antenna impedance values at the 3rd iteration.

https://doi.org/10.1017/S1759078719001375 Published online by Cambridge University Press

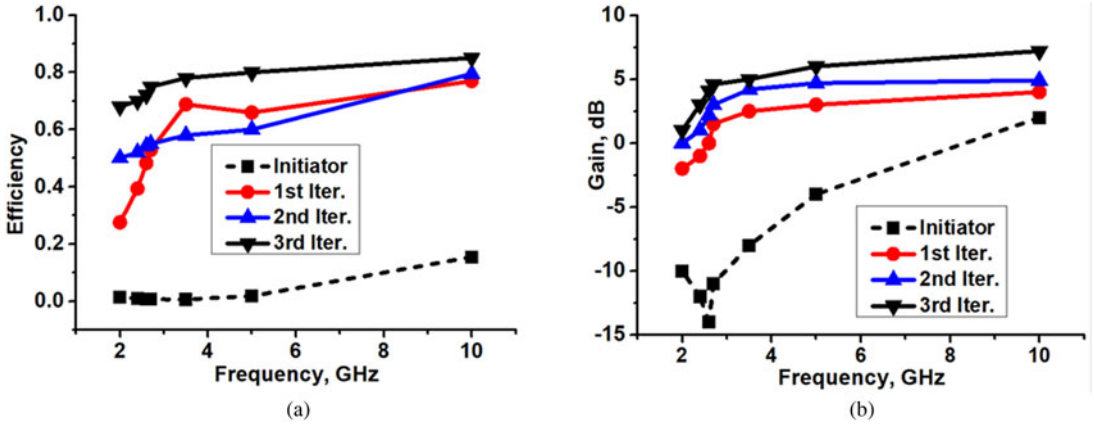

Fig. 5. Simulated efficiency and gain for all iterations. (a) Efficiency. (b) Gain.

bandwidth of 13 and 41%, respectively. In the third iteration, the values of the S_{11} decreased in the higher operating band, especially in the resonant frequency of 8.5 GHz. This finding is due to the addition of sunflower that changes the impedance of the proposed antenna in such a way that the values of the imaginary part (the solid red curve in Fig. 4) become almost equal to zero line (the red dashed line in Fig. 4). Thereafter, the values of real-part impedance (the black solid curve in Fig. 4) for the third iteration are closer to the input impedance of the excitation port (50 Ohms, the black dashed line), especially in the resonant frequency of 8.5 GHz.

The efficiency and gain values also improved during the configuration process of the antenna as is shown in Fig. 5. The total efficiency for the initiator antenna was less than 10% (dashed curve in Fig. 5(a)). Although the maximum efficiency values reached 70% at the 1st iteration, efficiency varied from 30 to 45% at lower bands (red curve in Fig. 5(a)). Efficiency tended to increase at the 2nd (blue curve in Fig. 5(a)) and 3rd (solid back curve in Fig. 5(a)) iterations. The same result was obtained for the gain values during the antenna configuration (Fig. 5(b)). The additional sunflower in high-order iteration increases the gain due to an increased effective area (A_e), as indicated in equations (2) and (3).

Diversity performance

Mutual coupling between the dual elements of the proposed MIMO fractal antenna was reduced by adding a strip line L with dimensions of 25×3 mm^2 to the outer edge of the ground plate for both elements (Fig. 2(d)). Figure 6 shows the effect of strip L on the values of mutual coupling ($S_{i,j}$), which were excessively reduced and became less than −25 dB (black curve in Fig. 5) compared with the red curve in Fig. 6.

The surface current distribution when element number 1 in the proposed MIMO fractal antenna was excited at 2.6 GHz is presented in Fig. 7. Most of the surface current was concentrated on the outer edge of antenna 1 and ground strip L (Fig. 7(a)). Meanwhile, Fig. 7(b) shows the amount of surface current at the narrow edge of antenna 2 when antenna 1 is excited in case the MIMO antenna has no ground strip L. This phenomenon occurs because the ground strip L is closer to antenna 1 than to antenna 2, leading to a higher excitation amount of surface current in the ground strip L than that in antenna 2. The same finding occurs when the second antenna is excited. Therefore, the

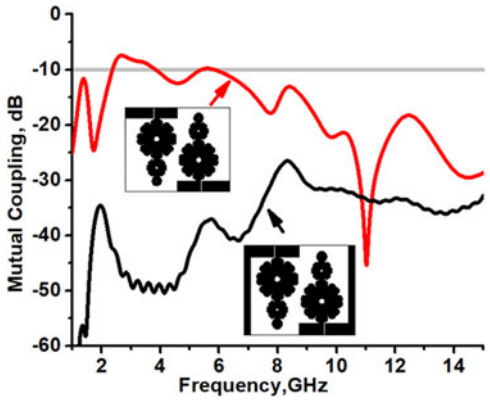

Fig. 6. Simulated mutual coupling between dual elements with and without sided ground strip L.

mutual coupling between dual radiation elements can be eliminated by adding ground strip L.

The difference between the envelop correlation coefficient (ECC) values for the cases of the MIMO antenna with (black curve) and without (red curve) ground strip L is clearly shown in Fig. 8(a), particularly in a frequency range of 2–3 GHz.

The total active reflection coefficient (TARC) for the 2×2 MIMO antenna can be calculated from the values of S-parameters (S_{11}, S_{21}, S_{12}, $S_{2,2}$) and the angle of exciting the 2nd port (α) by using equation (4) [1].

$$\text{TARC} = \frac{\sqrt{(|(S_{11} + S_{12}e^{j\alpha})|^2 + |(S_{21} + S_{22}e^{j\alpha})|^2)}}{\sqrt{2}} \quad (4)$$

The values of TARC for the proposed antenna improve dramatically by adding the ground strip L (the black curve in Fig. 8(b)). The ECC and TARC values are consistent with those in the study of surface current in Fig. 7 and the mutual coupling in Fig. 6, thereby proving that the mutual effect between the dual radiating elements can be reduced by adding strip L to the ground plate. Table 3 summarizes some of the specifications during the process of configuring the proposed MIMO sunflower fractal antenna.

https://doi.org/10.1017/S1759078719001375 Published online by Cambridge University Press

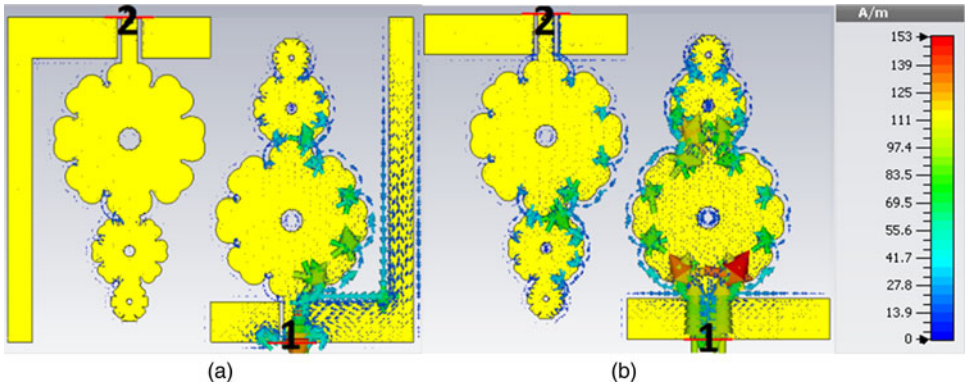

Fig. 7. Surface current when antenna1 excited at 2.6 GHz. (a) With ground side strip. (b) Without ground side strip.

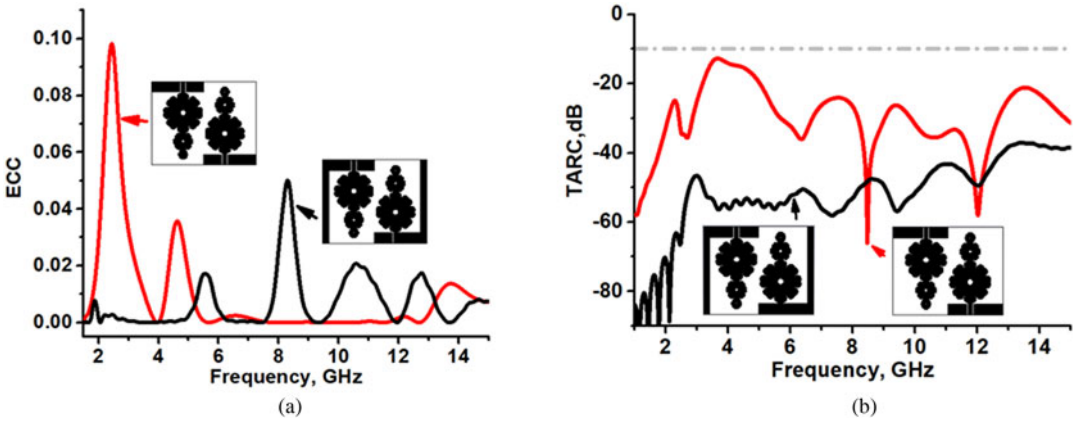

Fig. 8. Simulated ECC and TARC for the proposed antenna with and without ground strip *L*. (a) ECC. (b) TARC.

Table 3. Specifications at all iterations

Iteration	BW (GHz)	Gain (dB)	Efficiency (%)	State
Initiator	–	−15 to 0	0–10	Poor radiation properties
1st	(2.6–7.1) (7.5–12)	−3 to 2	30–70	Low gain & efficiency at lower band
2nd	(2.5–3) (5.5–12)	0–5	50–75	The operating band width didn't support 3G & WLAN applications
3rd	(2.1–2.74) (5–12)	1–7	70–85	Optimum

Fig. 9. Prototypes of the sunflower MIMO fractal antenna. (a) With ground strip *L*. (b) Without ground strip *L*.

https://doi.org/10.1017/S1759078719001375 Published online by Cambridge University Press

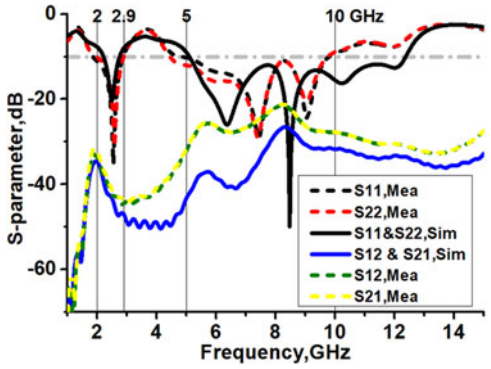

Fig. 10. Simulated (solid curves) and measured (dashed curves) reflection coefficients.

Measurements and results

Figure 9 presents the prototype of the MIMO fractal antenna, whereas Fig. 10 shows the measured and simulated reflection coefficients. The measured values of the impedance bandwidth for the 1st element (S_{11}) expanded at the 1st bandwidth within the frequency range of 1.8–2.9 GHz compared with the simulated values of 2.1–2.74 GHz. The measured 2nd bandwidth was compressed to the frequency range of 4.8–9.8 GHz compared with the simulated result of 5–12 GHz. The measured dual operating bands for the 2nd element (S_{22}) are 2–2.8 and 4.4–10 GHz, whereas the simulated impedance bandwidths for the 2nd element are 2.1–2.74 and 5–12 GHz. The phenomena of mismatching between the measured and the simulated impedance bandwidths (especially at the upper operating band) was occurred due to the impurity of some materials used in the prototype and the impedance of the connectors which varies dramatically at high-operating frequencies. The measured mutual coupling values between the dual radiating elements varied from −45 to−35 dB and −35 to −25 dB at the 1st and the 2nd operating bands, respectively. Figure 10 shows some discrepancies between the measured (dashed yellow and blue curves) and simulated (solid blue curve) mutual coupling values especially at the upper

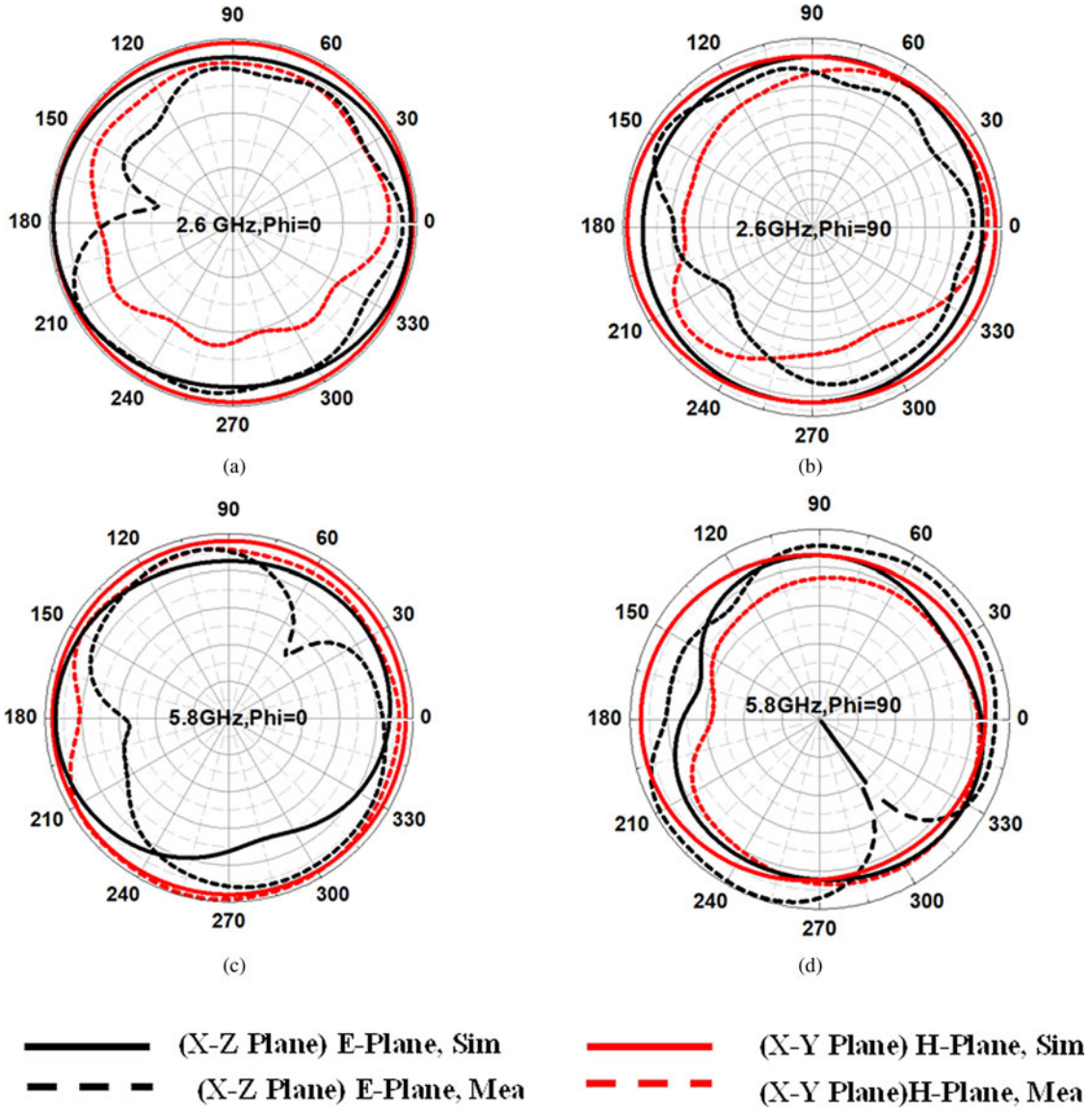

Fig. 11. Normalized radiation patterns in the *E*-plane (*X*–*Z* plane) and *H*-plane (*X*–*Y* plane). (a) At 2.6 GHz, $\emptyset = 0^\circ$. (b) At 2.6 GHz, $\emptyset = 90^\circ$. (c) At 5.8 GHz, $\emptyset = 0^\circ$. (d) At 5.8 GHz, $\emptyset = 90^\circ$.

https://doi.org/10.1017/S1759078719001375 Published online by Cambridge University Press

operating band due to use a defected-ground in the simulation. While in practical, the ground for all ports connected to a common point [34].

Figure 11 presents the normalized radiation patterns at resonant frequencies of 2.6 GHz for LTE communication and 5.8 GHz for WLAN and WiMAX communication. An acceptable agreement was attained between the simulated (solid curves) and measured (dashed curves) radiation patterns in the *E*-plane (black curves) and *H*-plane (red curves) when $\emptyset = 0$ and 90°, respectively. The measured radiation pattern in the *E* plane at 5.8 GHz when $\emptyset = 0^{\circ}$ has two lobes at angles of 110 and 300°, similar to number 8 (Fig. 11(c), the black dashed curve).

Figure 11(d) shows an apple shape, which presents the measured radiation pattern in the *E* plane when $\emptyset = 90^{\circ}$ in the frequency of 5.8 GHz; the pattern is null at 300°. The directivity *D* increases with increasing frequency (reducing the wavelength λ), as shown in equation (2).

Figure 12 shows some discrepancies between the simulated (read curves) and measured (black curves) TARC values (especially at the band of 5–10 GHz) of the proposed antenna when $\alpha = 0$ and 90°. This finding is due to the impurity of some materials used in the prototype and soldering. The antenna has low-mutual coupling due to the ground strip *L*, especially in the low-operating band (2–2.9 GHz) when $\alpha = 0°$ (the black solid curve).

The measured and simulated values of efficiency and gain are illustrated in Fig. 13. The measured gain (dashed blue curve) of the proposed antenna varied from 1 dB at 2 GHz to 6 dB at 10 GHz, whereas the measured efficiency (dashed black curve) varied between 65% at 2 GHz and 85% at 10 GHz.

The CCL characterizes the quality of the MIMO system which can be calculated according to equation (5) [19]:

$$\mathrm{CCL} = -10\log_2 \det(\rho) \tag{5}$$

where ρ is the correlation matrix of the receiving antenna and can be calculated as:

$$\rho = \begin{bmatrix} \rho_{11} & \rho_{12} \\ \rho_{21} & \rho_{22} \end{bmatrix},\ \rho_{ii} = 1 - (|s_{ii}|^2 + |s_{ij}|^2) \text{ and } \rho_{ij} = (s_{ii}\, s_{ij})^2 + (s_{ji}\, s_{ij})^2,\ i, j = 1 \text{ or } 2$$

Figure 14 presents the measured and simulated CCL values. The dashed curve in Fig. 14 shows that the measured values of the CCL for the proposed sunflower MIMO fractal antenna did not overstep 0.4 b/s/Hz at a lower operating band (2–2.9 GHz) and varied between 0.15 and 0.35 b/s/Hz at a upper operating band (5–10 GHz). Therefore, the sunflower MIMO fractal antenna has low-CCL values that can be used in modern digital communication devices.

The specifications of the MIMO sunflower fractal antenna are better than those of the previous MIMO fractal antennas investigated in [3, 8, 9, 17, 18, 19, 26, 27] due to the following reasons.

(1) None of the previous MIMO fractal antennas with the same size ($40 \times 50 \times 0.8$ mm^3) can support 3G, LTE (4G), WLAN (IEEE 802.11n and IEEE 802.11ac), WiMAX (IEEE 802.16), and 5G (5–6 GHz) communication networks.
(2) The mutual coupling between the antennas reduced 20 dB by inserting a strip line into the outer edges of the ground plate.
(3) None of the previous MIMO antennas with the same size ($40 \times 50 \times 0.8$ mm^3) have the same mutual coupling (from −45 to −25 dB), CCL (0.15–0.4 b/s/Hz), efficiency (65–85%), and gain (1–6 dBi).
(4) The MIMO sunflower fractal antenna exhibits a novel design with a low profile etched on a low-cost and commercial FR-4 substrate.

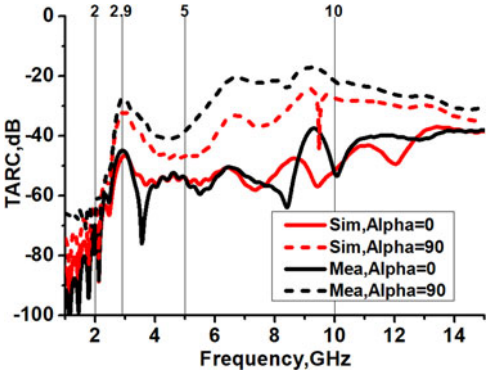

Fig. 12. Measured and simulated TARC for$\alpha = 0$ and 90°.

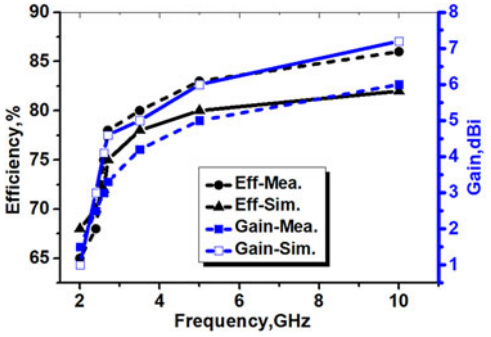

Fig. 13. Simulated (solid curves) and measured (dashed curves) values of the gain and the efficiency of the MIMO antenna.

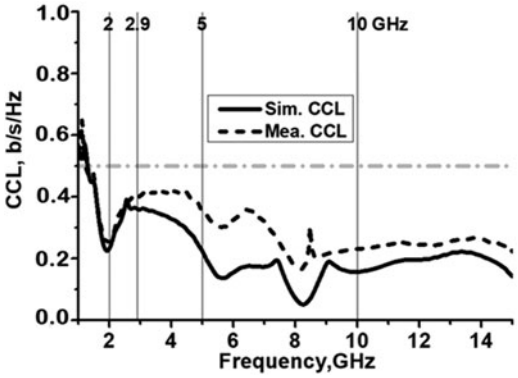

Fig. 14. Simulated and measured CCL for the sunflower MIMO fractal antenna.

Conclusion

This work designed a novel MIMO fractal antenna that can support many modern wireless communication applications, such as: 3G, LTE (2.6 GHz), WLAN (IEEE 802.11n and IEEE 802.11ac), WiMAX (2.4 GHz/5 GHz), ISM (2.4 GHz/5 GHz), and 5G (5–6 GHz). Furthermore, the MIMO sunflower fractal antenna has low-mutual coupling, low-CCL, acceptable values of gain and efficiency, and small size. The characteristics of the designed

https://doi.org/10.1017/S1759078719001375 Published online by Cambridge University Press

antenna make it suitable for many communication portable devices.

Acknowledgement. Special thanks to Mr. Omar Almukhtar T. Najim, Communication Engineering Depart., Al-Ma'moon University College and Centre of Advanced Electronic and Communication Engineering, (UKM), Malaysia.

References

1. **Abed AT** (2019) *Fractal and Slot Antennas for Portable Communication Devices*, 1st Edn. Saarbrücken, Germany: Lab Lambert for Academic Publication.
2. **Sharma Y, Debdeep S, Kushmanda S and Kumar VS** (2017) Three-element MIMO antenna system with pattern and polarization diversity for WLAN applications. *IEEE Antennas and Wireless Propagation Letters* **16**, 1163–1166.
3. **Peristerianos A, Argiris T, Anastasios GK and Theodoros K** (2016) Dual-band fractal semi-printed element antenna arrays for MIMO applications. *IEEE Antennas and Wireless Propagation Letters* **15**, 730–733.
4. **Jehangir SS and Sharawi MS** (2017) A miniaturized UWB biplanar Yagi-like MIMO antenna system. *IEEE Antennas and Wireless Propagation Letters* **16**, 2320–2323.
5. **Hussain R and Sharawi MS** (2017) Annular slot-based miniaturized frequency-agile MIMO antenna system. *IEEE Antennas and Wireless Propagation Letters* **16**, 2489–2492.
6. **Ghalib A and Sharawi MS** (2017) TCM analysis of defected ground structures for MIMO antenna designs in mobile terminals. *IEEE Access* **5**, 19680–19692.
7. **Park S-J, Myung-Hun J, Kyung-Bin B, Dong-Chan K and Laxmikant M** (2017) Performance comparison of 2 × 2 MIMO antenna arrays with different configurations and polarizations in reverberation chamber at millimeter-waveband. *Transactions on Antennas and Propagation* **65**, 6669–6678.
8. **Rajkumar S, Narayanaswamy VS, Sharada M and Krishnasamy TS** (2017) Heptaband swastik arm antenna for MIMO applications. *IET Microwaves, Antennas & Propagation* **11**, 1255–1261.
9. **Saeed Khan M, Antonio DC, Adnan I, Raed MS and Dimitris EA** (2017) Ultra-compact dual-polarised UWB MIMO antenna with meandered feeding lines. *IET Microwaves, Antennas and Propagation* **11**, 997–1002.
10. **Deng JY, Jin YL, Luyu Z and LiXin G** (2017) A dual-band inverted-F MIMO antenna with enhanced isolation for WLAN applications. *IEEE Antennas and Wireless Propagation Letters* **16**, 2270–2273.
11. **Ramachandran A, Sumitha M, Vivek R and Vasudevan K** (2017) A compact triband quad-element MIMO antenna using SRR ring for high isolation. *IEEE Antennas and Wireless Propagation Letters* **16**, 1409–1412.
12. **Hussain R, Ali TA, Symon KP and Mohammad SS** (2016) Compact 4G MIMO antenna integrated with a 5G array for current and future mobile handsets. *IET Microwaves, Antennas and Propagation* **11**, 271–279.
13. **Li G, Huiqing Z, Zhihui MA, Changhong L, Rongdao YU and Sheng L** (2014) Isolation-Improved dual-band MIMO antenna array for LTE/WiMAX Mobile terminals. *IEEE Antennas and Wireless Propagation Letters* **13**, 1128–1131.
14. **Mao C-X and Chu Q-X** (2014) Compact Co-radiator UWB-MIMO antenna with dual polarization. *Transactions on Antennas and Propagation* **62**, 4474–4480.
15. **Toktas A and Akdagli A** (2014) Wideband MIMO antenna with enhanced isolation for LTE, WiMAX and WLAN mobile handsets. *Electronics letters* **50**, 723–724.
16. **Brzezina G, Amir AB, Amir G, John S and Alex V** (2013) Design and analysis of a low-profile directive antenna array for multi-element terminals. *IET Microwaves, Antennas and Propagation* **8**, 611–620.
17. **Tripathi S, Mohan A and Yadav S** (2015) A compact Koch fractal UWB MIMO antenna with WLAN band-rejection. *IEEE Antennas and Wireless Propagation Letters* **14**, 1565–1568.
18. **Peristerianos A, Argiris T, Anastasios GK, Theodoros K and Katherine S** (2016) Dual-band fractal semi-printed element antenna arrays for MIMO applications. *IEEE Antennas and Wireless Propagation Letters* **15**, 1573–1573.
19. **Choukiker YK, Sharma SK and Behera SK** (2014) Hybrid fractal shape planar monopole antenna covering multiband wireless communications with MIMO implementation for handheld mobile devices. *IEEE Transactions on Antennas and Propagation* **26**, 1483–1488.
20. **Dhar SK, Sharawi MS, Hammi O and Ghannouchi FM** (2016) An active integrated ultra-wideband MIMO antenna. *IEEE Transactions on Antennas and Propagation* **64**, 1573–1578.
21. **Kang L, Hui L, Xinhuai W and Xiaowei S** (2015) Compact offset microstrip-fed MIMO antenna for band-notched UWB applications. *IEEE Antennas and Wireless Propagation Letters* **14**, 1754–1758.
22. **Zhang S and Pedersen GF** (2016) Mutual coupling reduction for UWB MIMO antennas with a wideband neutralization line. *IEEE Antennas and Wireless Propagation Letters* **15**, 166–169.
23. **Zhang Y and Wang P** (2015) Single ring two-port MIMO antenna for LTE applications. *Electronics Letters* **52**, 998–1000.
24. **Wang SM, Lih-Tyng H, Cho-Jung L, Chung-Yi H and Fa-Shian C** (2016) MIMO antenna design with built-in decoupling mechanism for WLAN dual-band applications. *Electronics Letters* **51**, 966–968.
25. **Yang Y, Chu Q and Mao C** (2016) Multiband MIMO antenna for GSM, DCS, and LTE indoor application. *IEEE Antennas and Wireless Propagation Letters* **15**, 1573–1157.
26. **Yang L, Li T and Yan S** (2016) Highly compact MIMO antenna system for LTE/ISM applications. *International Journal of Antennas and Propagation* **2015**, 1–10.
27. **Abed AT** (2018) Highly compact size serpentine-shaped multiple-input–multiple-output fractal antenna with CP diversity. *IET Microwaves, Antennas and Propagation* **12**, 636–640.
28. **Hussain R, Muhammad UK and Mohammad SS** (2018) An integrated dual MIMO antenna system with dual-function GND-plane frequency-agile antenna. *IEEE Antennas and Wireless Propagation Letters* **17**, 142–145.
29. **Sui J and Wu K-L** (2018) Self-curing decoupling technique for two inverted-F antennas with capacitive loads. *IEEE Transactions on Antennas and Propagation* **66**, 1093–1101.
30. **Ding K, Cheng G, Dexin Q and Qin Y** (2017) Compact broadband MIMO antenna with parasitic strip. *IEEE Antennas and Wireless Propagation Letters* **16**, 2349–2353.
31. **Abed AT and Jawad AM** (2019) Compact size MIMO Amer fractal slot antenna for 3G, LTE (4G), WLAN, WiMAX, ISM and 5G communications. *IEEE Access* **7**, 125542–125551.
32. **Abed AT, Mandeep JS and Mohamed TI** (2018) Compact fractal antenna circularly polarised radiation for Wi-Fi and WiMAX communications. *IET Microwaves, Antennas and Propagation* **12**, 2218–2224.
33. **Balanis CA** (2005) *Antenna Theory: Analysis and Design*, 3rd Edn, John Wiley & Sons, Inc., USA.
34. **Sharawi MS** (2017) Current misuses and future prospects for printed multiple-input, multiple-output antenna systems. *IEEE Antennas and Propagation Magazine* **59**, 162–170.

Amer Tawfeeq Abed received a degree in Electrical Engineering from College of Engineering, University of Baghdad, 1984. He has obtained his master's in Communication Engineering from University of TENAGA, Malaysia and his Ph.D. from UKM, Malaysia. He has wide experience in designing the RF circuit and antennas. Dr. Abed has published 25 papers in ISI journals and 2 books about antenna design. He has reviewed more than 30 articles in IET and IEEE journals. Dr. Abed is a member of the European Microwave Association (EMA) and IEEE. Currently, he is a lecturer in Communication Engineering Department, Al-M'mamon University College, Baghdad-Iraq.

https://doi.org/10.1017/S1759078719001375 Published online by Cambridge University Press